

Experimental *n*-Hexane-Air Expanding Spherical Flames

Stephanie A. Coronel¹, Simon Lapointe¹, Rémy Mével^{2,3}, Nabih Chaumeix⁴, Joseph E. Shepherd¹

¹California Institute of Technology, Pasadena, CA, USA

²Center for Combustion Energy, ³Dept. of Automotive Engineering, Tsinghua University

⁴ICARE, CNRS-INSIS, Orléans, France

1 Introduction

During aircraft operation, the pressure within the fuel tank and other areas potentially containing flammable mixtures varies between 20 and 100 kPa. To assess the risk of potential ignition hazards and flammability in fuel tank ullage or flammable leakage zones, it is necessary to characterize properties such as the laminar burning rate of fuel-air mixtures over a wide range of initial pressures and temperatures. *n*-Hexane has been extensively used at the Explosion Dynamics Laboratory as a single component surrogate of kerosene; *n*-hexane exhibits a relatively high vapor pressure which facilitates experimenting at ambient temperature. A limited number of studies have been found on the laminar burning speed. [1] measured the laminar burning speed of *n*-hexane-air mixtures at ambient conditions using the counterflow twin flame technique. [2] used pressure traces from spherically expanding flames to determine the laminar burning speed of *n*-hexane-air mixtures at an initial temperature and pressure of 450 K and 304 kPa, respectively. [3] reported experimental measurements using spherically expanding flames at an initial temperature of 353 K and an initial pressure range of 100 – 1000 kPa. [4] used the counterflow burner technique to measure the laminar burning speed of *n*-hexane-air mixtures at an initial temperature and pressure of 353 K and 100 kPa, respectively. In contrast to previous work, the present study focuses on initial conditions below atmospheric pressure in order to simulate aircraft fuel tank conditions. Additionally, this study investigates the effect of initial temperature at sub-atmospheric conditions to simulate elevated temperature conditions in the fuel tank ullage or flammable leakage zones.

2 Experimental Setup and Methodology

Two laboratories participated in the present study to perform experiments over a wide range of initial temperature conditions: the EDL at the California Institute of Technology (Caltech) and ICARE-Centre National de la Recherche Scientifique (CNRS) Orléans. At the EDL, the experiments were performed in a 22 L stainless steel combustion vessel. Parallel flanges were used to mount electrodes for the ignition system and windows for optical access. The mixtures were ignited by a 300 mJ electric spark generated between two 0.4 mm in diameter tungsten electrodes separated by a distance of 2 – 4 mm. A high-speed camera (Phantom v711) was used to record the flame propagation observed using Schlieren visualization and shadowgraphy at a rate of 10,000 frames per second with a resolution of 512 px × 512 px. The experiments conducted at ICARE-CNRS were performed in a stainless steel spherical bomb consisting of two concentric spheres;

the internal sphere had an inner diameter of 476 mm. The mixtures were ignited by electric sparks with a nominal energy of 1.82 mJ. Schlieren visualization was used with a high-speed camera (Phantom V1610) at a rate of 25, 000 frames per second with a resolution of 768 px \times 768 px.

The flame radius as a function of time was extracted from the experimental images of expanding spherical flames using algorithms implemented in Matlab, including an edge detection operator [5]. The images of the spherically propagating flames were processed by first applying a mask over each image to remove the background (electrodes). Edge detection was then used to identify the expanding flame edge. An ellipse was fitted to the detected flame edge; the ellipse parameters were then used to obtain an equivalent radius, R_f . For the majority of the experimental images, the flame sphericity (semi-major axis divided by the semi-minor axis) was approximately equal to 1. The nonlinear model [6], shown in Eq. 1, for spherical flame speed as a function of curvature was used to extract the unstretched flame speed, S_b^0 , and Markstein length, L_B .

$$\frac{S_b}{S_b^0} \ln \left(\frac{S_b}{S_b^0} \right) = -2 \frac{L_B}{R_f} . \quad (1)$$

Numerical integration was used to extract the flame properties from Eq. 1. The unstretched burning speed, S_u^0 was obtained through $S_u^0 = S_b^0/\sigma$, where σ is the expansion ratio defined as $\sigma = \rho_u/\rho_b$, where ρ_u and ρ_b are the unburnt and burnt gas densities, respectively. For the remainder of this study, the unstretched burning speed will be referred to as the laminar burning speed.

3 Experimental Results

Experimental laminar burning speeds at an initial temperature of 296 K and pressure of 100 kPa are shown in Fig. 1 (a) along with results previously obtained by [1]. The uncertainty in the laminar burning speeds is on average 6%, the value is based on previous estimates made by [5] who used the same flame detection algorithms employed in the present study. Figure 1 also shows 1D freely propagating flame calculations performed using FlameMaster [7] with three different chemical kinetic mechanisms: CaltechMech [8], JetSurF [9], and the mechanism of [10] (referred to as Mével in this study). Further details on mechanism description and performance are provided in Section 4. A Mann-Whitney-Wilcoxon (MWW) RankSum test indicated that the differences in the two laminar burning speed distributions shown in Fig. 1 (a) were not statistically significant. The evolution of the laminar burning speed as a function of equivalence ratio was studied at a nominal initial temperature and pressure of 300 K and 50 kPa, respectively. Figure 1 (b) shows the laminar burning speed obtained at initial pressures of 100 kPa and 50 kPa. The MWW RankSum test indicated that the differences in the laminar burning speed distributions at 100 kPa and 50 kPa were not statistically significant.

The effect of initial pressure on the laminar burning speed was investigated at $\Phi = 0.90$ and a nominal initial temperature of 357 K. The experimental laminar burning speed is shown in Fig. 2 (a) along with experimental results obtained by [3] at initial pressures of 100 – 1000 kPa and an initial temperature of 353 K. The laminar burning speed decreases with increasing initial pressure, 20% between 50 and 100 kPa and 53% between 50 and 1000 kPa at nominal initial temperatures of 353 and 357 K. The pressure dependence on the laminar burning speed can be fit to a power law: $S_u^0(P) = 128 \times P^{-0.24}$, where P has units of kPa. The corresponding standard deviations for the pre-exponential and exponent are 12 and 0.02, respectively. The effect of initial temperature was studied at an initial pressure of 50 kPa and three equivalence ratios, $\Phi = \{0.90, 1.10, 1.40\}$. The laminar burning speed is shown in Fig. 2 (b). At initial

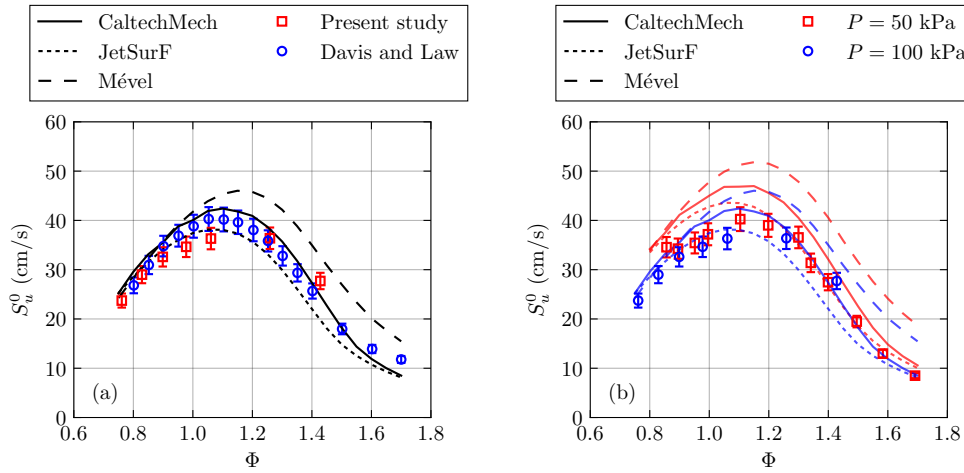


Figure 1: Experimental laminar burning speed as a function of Φ at a (a) nominal initial temperature and pressure of 300 K and 100 kPa, respectively, and (b) nominal initial pressures of 50 kPa and 100 kPa and nominal initial temperature of 300 K; numerical calculations also shown.

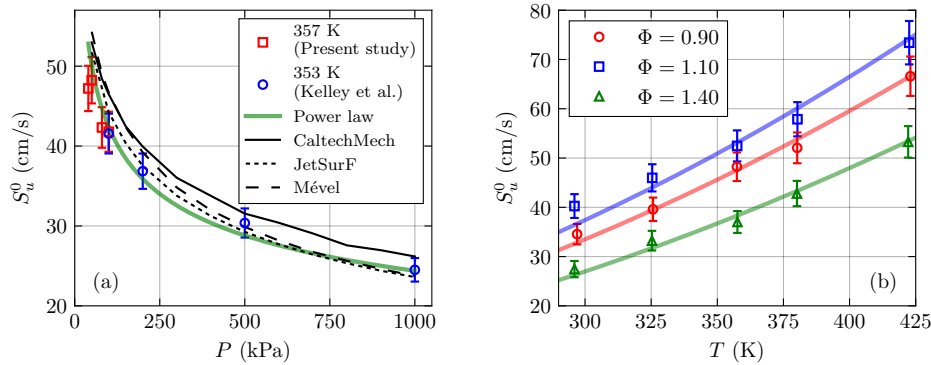


Figure 2: Experimental laminar burning speed as a function of (a) initial pressure at a nominal initial temperature of 353 and 357 K, along with numerical calculations, and (b) as a function of initial temperature at a nominal initial pressure of 50 kPa and $\Phi = 0.9, 1.1, \text{ and } 1.4$ (the solid lines correspond to $S_u^0 \sim T^2$).

temperatures of 296 K to 422 K, the laminar burning speed increases by approximately 93%, 82%, and 94% for $\Phi = 0.90, \Phi = 1.10, \text{ and } \Phi = 1.40$, respectively. There is a difference between the laminar burning speeds distributions shown for $\Phi = \{0.90, 1.10, 1.40\}$. Each distribution can be fit to a power law $S_u^0 \sim T^2$ shown in Fig. 2 (b).

Figure 3 (a) shows the variation of the Markstein length with equivalence ratio at an initial temperature and pressure of 296 K and 50 kPa, respectively. Lean and rich mixtures exhibit positive and negative Markstein lengths, respectively. The transition from positive to negative Markstein length occurs at $\Phi \approx 1.3$. This trend is consistent with previous Markstein length results obtained for C_5 to C_8 *n*-alkane-air mixtures [3]. Figure 3 shows the Markstein length extrapolated using a linear and nonlinear dependence of the stretched flame speed on stretch rate. The linear dependence on stretch rate is given by $S_b = S_b^0 - L_B \kappa$. It is evident from the figure that deviations of the nonlinear L_B from the linear L_B occur for both rich and lean *n*-hexane-air mixtures. Figure 3 (b) shows the product of the Markstein number, Ma_{linear} (obtained via

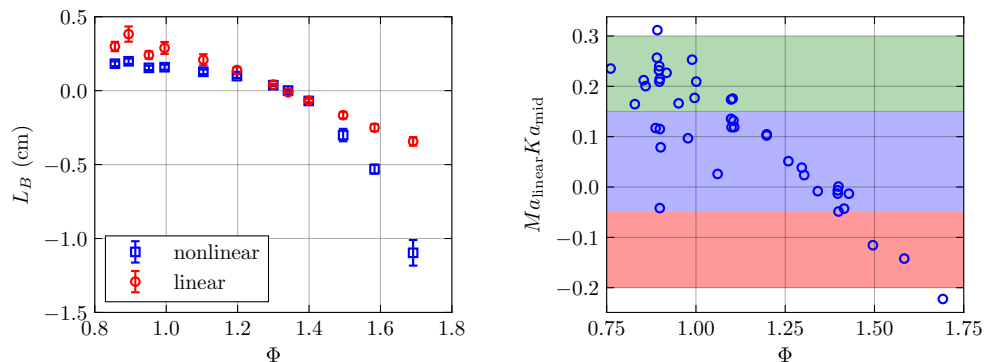


Figure 3: (a) Evolution of the Markstein length as a function of Φ at a nominal initial temperature and pressure of 296 K and 50 kPa, respectively, using linear and nonlinear extrapolations and (b) $Ma_{\text{linear}}Ka_{\text{mid}}$ as a function of Φ for initial temperatures and pressures of 296 K to 380 K, and 40 kPa to 100 kPa, respectively.

the linear extrapolation method), and the Karlovitz number, Ka_{mid} (evaluated at the mid-point of the flame radii data), as a function of the mixture equivalence ratio. The product is suggested by [11] as a method to evaluate the uncertainty of the extrapolation method. In Fig. 3 (b), the blue, green, and red regions have extrapolation uncertainties of $\leq 5\%$, 5 – 12%, and 5 – 40%, respectively. The points lying in the red region correspond to rich conditions at a nominal initial temperature and pressure of 296 K and 50 kPa, respectively. Under rich conditions, the flame instability is more intense and complicates the accurate determination of the laminar burning speed.

4 Modeling Results

The 1D freely propagating flame calculations performed with FlameMaster [7] used the chemical kinetic mechanisms of CaltechMech [8], JetSurF [9], and Mével [10]. The calculations neglected Soret and Dufour effects, and a mixture-averaged formulation was used for the transport properties. [4] showed that using a multicomponent transport coefficient formulation rather than mixture-averaged transport properties resulted in a 1 cm/s increase in the calculated laminar burning speeds of C_5 - C_{12} *n*-alkane mixtures. A study by [12] found that accounting for Soret effects resulted in a maximum of 1 – 2% increase in the laminar burning speed of *n*-heptane-air flames at and near stoichiometric conditions. Finally, [13] showed that for C_3 laminar premixed flames, the effect of excluding Dufour effects was negligible.

Figures 1 and 2 show comparisons between the experimental and calculated laminar burning speeds. Additional comparisons are made with experimental data from [4] and [3]. Visual inspection of the figures indicates that the chemical kinetic mechanism of Mével cannot predict the laminar burning speed with appropriate accuracy. On the other hand, the predictions of CaltechMech and JetSurF appear to be more accurate; however, it is difficult to ascertain qualitatively which mechanism performs best. The performance of each mechanism is quantitatively evaluated using the root-mean-squared error formulation, $RMSE = \sqrt{1/N \sum_{i=1}^N (S_{\text{calc}}^{(i)} - S_{\text{exp}}^{(i)})^2}$, where S_{calc} and S_{exp} are the calculated and experimental laminar burning speeds, respectively, N is the number of points for each experimental data set, and i corresponds to the i^{th} point in a data set. The RMSE is calculated for the experimental data sets shown in Table 1. A total of 87 points are used to evaluate the performance of each mechanism, shown in Fig. 4.

Table 1: Experimental data sets of laminar burning speed used for the RMSE calculation to evaluate the performance of the chemical kinetic mechanisms used in the present study.

Data	Reference	P (kPa)	T (K)	Φ	N
A	Present study	100	296	0.76 – 1.42	7
B	[1]	100	300	0.85 – 1.70	16
C	[4]	100	353	0.75 – 1.50	10
D	[3]	100	353	0.75 – 1.70	19
E	Present study	50	296	0.86 – 1.69	12
F	Present study	50	297 – 423	0.9	5
G	Present study	50	296 – 422	1.1	5
H	Present study	50	296 – 422	1.4	5
I	Present study	40 – 100	357	0.9	4
J	[3]	100 – 1000	353	0.9	4

Overall, JetSurF yields the smallest RMSE values for almost all the experimental conditions presented in this study and previous studies. The RMSE based on set A ($P = 100$ kPa and $T = 300$ K) is the same between JetSurF (RMSE = 3.5 cm/s) and CaltechMech; the RMSE based on set B (experiments performed by [1]) is smaller, by approximately 19%, for CaltechMech (RMSE = 2.1 cm/s) than JetSurF (RMSE = 2.6 cm/s). For almost all the experimental conditions presented, Mével (RMSE = 2.9 – 14.8 cm/s) yields the largest RMSE values when compared to those obtained with JetSurF and CaltechMech. The RMSE based on set J (experiments performed by [3]) is smaller, by approximately 6%, for Mével (RMSE = 2.9 cm/s) than CaltechMech (RMSE = 3.1 cm/s). When considering the RMSE of sets F, G, and H, ($P = 50$ kPa and $T \sim 300 - 422$ K) CaltechMech performs best at rich conditions ($\Phi = 1.4$); the RMSE for set H is 5.0 cm/s, approximately 24% and 38% smaller than the RMSE obtained with sets F ($\Phi = 0.9$) and G ($\Phi = 1.1$), respectively. For JetSurF, set H also has the smallest RMSE (1.8 cm/s) when compared to sets F (RMSE = 4.7 cm/s) and G (RMSE = 3.9 cm/s). In regard to the mechanism of Mével, the leaner data set F has the smallest RMSE (7.9 cm/s) when compared to the close to stoichiometric and rich conditions of sets G (RMSE = 13.1 cm/s) and H (RMSE = 14.8 cm/s), respectively. The mean RMSE across the conditions presented in Table 4 is 5.0 cm/s, 2.8 cm/s, and 9.0 cm/s for CaltechMech, JetSurF, and Mével, respectively. Based on a mean RMSE representation of the model performance, JetSurF is the appropriate chemical kinetic mechanism to use when calculating the laminar burning speed of *n*-hexane-air mixtures across a wide range of conditions.

5 Summary

n-Hexane-air mixtures were characterized through experimental measurements and calculations of the laminar burning speed. The laminar burning speed was obtained by using a nonlinear methodology. The effect of equivalence ratio, temperature, and pressure on the laminar burning speed was investigated experimentally by varying the equivalence ratio $\Phi = 0.62 - 1.60$, the initial temperature from 296 K to 422 K, and the initial pressure from 50 kPa to 100 kPa. The laminar burning speed was observed to increase as pressure decreases ($T = 357$ K) and as temperature increases. It was also shown that the laminar burning speed increases at comparable rates as temperature increases for mixtures at $\Phi = \{0.90, 1.10, 1.40\}$. The predictive capabilities of three chemical kinetic mechanisms from the literature were quantitatively evaluated

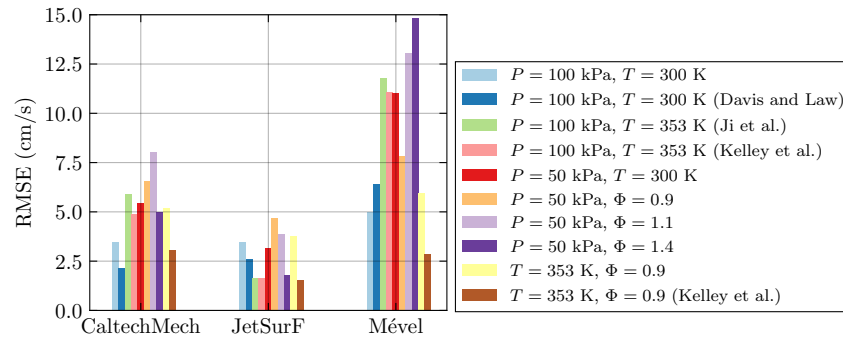


Figure 4: Root-mean-squared-error (RMSE) of the calculated laminar burning speeds.

using the present experimental data and those from the literature. Based on a RMSE analysis, it was shown that JetSurF was the most appropriate mechanism for modeling the laminar burning speed of *n*-hexane-air mixtures over a wide range of mixture compositions and thermodynamic conditions.

References

- [1] Davis SG, Law CK. (1998). *Combust. Sci. Technol.* 140: 427.
- [2] Farrell J, Johnston R, Androulakis I. (2004). *SAE Tech. Paper.* 2004-01-2936.
- [3] Kelley AP, Smallbone AJ, Zhu DL, Law CK. (2011). *P. Combust. Inst.* 33: 963.
- [4] Ji C, Dames E, Wang Y, Wang H, Egolfopoulos FN. (2010). *Combust. Flame.* 157: 277.
- [5] Mével R, Lafosse F, Chaumeix N, Dupré G, Paillard C-E. (2009). *Int. J. Hydrogen Energ.* 34(21): 9007.
- [6] Ronney PD, Sivashinsky GI. (1989). *SIAM J. Appl. Math.* 49: 1029.
- [7] Pitsch H (1998). *FlameMaster*, a C++ computer program for 0D combustion and 1D laminar flame calculations.
- [8] Blanquart G, Pepiot-Desjardins P, Pitsch H. (2016). *Combust. Flame.* 156(3): 588
- [9] Wang H. et al. (2010). A high-temperature chemical kinetic model of *n*-alkane (up to *n*-dodecane), cyclohexane, and methyl-, ethyl-, *n*-propyl and *n*-butyl-cyclohexane oxidation at high temperatures, *JetSurF* version 2.0.
- [10] Mével R, Chatelain K, Boettcher PA, Shepherd JE. (2014). *Fuel.* 126: 282.
- [11] Wu F, Liang W, Chen Z, Ju Y, Law CK. (2015). *P. Combust. Inst.* 35(1): 663.
- [12] Xin Y, Sung C-J, Law CK. (2012). *Combust. Flame.* 159(7): 2345.
- [13] Bongers H, Goey LPHD. (2003). *Combust. Sci. Technol.* 175(10): 1915.